

A Measurement of Cubic-Order Primordial Non-Gaussianity (g_{NL} and τ_{NL}) With WMAP 5-Year Data

Joseph Smidt*,¹ Alexandre Amblard,¹ Asantha Cooray,¹ Alan Heavens,² Dipak Munshi,^{2,3} and Paolo Serra¹

¹*Center for Cosmology, Department of Physics and Astronomy,
University of California, Irvine, CA 92697, USA*

²*Scottish Universities Physics Alliance (SUPA), Institute for Astronomy,
University of Edinburgh, Blackford Hill, Edinburgh EH9 3HJ, UK*

³*School of Physics and Astronomy, Cardiff University, CF24 3AA*

(Dated: May 29, 2022)

We measure two higher-order power spectra involving weighted cubic and squared temperature anisotropy maps from WMAP 5-year data to study the trispectrum generated by primordial non-Gaussianity. Using these measurements and Gaussian and noise simulations, we constrain the cubic order non-Gaussianity parameters, f_{NL}^2 , or equivalently τ_{NL} , and g_{NL} . With V+W-band data out to $l_{\text{max}} = 600$, we find $-631 < \sqrt{f_{\text{NL}}^2} < 717$ and $-3.80 < g_{\text{NL}}/10^6 < 3.88$ jointly at 95% confidence level. We improve the previous COBE-based limit on $\tau_{\text{NL}} < 10^8$ by roughly three orders of magnitude to $-3.2 < \tau_{\text{NL}}/10^5 < 3.3$ at 95% confidence level with WMAP.

Introduction.—The inflationary paradigm has deservedly become a cornerstone of modern cosmology [1–3]. Inflation solves the flatness, horizon and the monopole problems of the standard Big-Bang cosmology. Furthermore, inflation is the prevailing paradigm related to the origin of density perturbations that gave rise to the large-scale structure we see today. It posits that a nearly exponential expansion stretched space in the first moments of the early universe and promoted microscopic quantum fluctuations to perturbations on cosmological scales today [4–7]. Inflation makes detailed predictions for key statistical features of these fluctuations. These predictions have now begun to be tested by a range of cosmological observations, including cosmic microwave background (CMB) temperature anisotropy and polarization.

In the standard scenario, inflation is driven by a single scalar field whose potential energy dominates its kinetic energy. This “slow-roll” situation leads to an exponential expansion of the cosmic spacetime via the Einstein equations coupled to a scalar field. In order to maintain a slow roll, the scalar field must have minimal self interactions. Such a non-interacting field has the statistical feature that its fluctuations are Gaussian. If a departure from Gaussianity is detected in these primordial fluctuations, it will signal that the standard slow roll paradigm of a single scalar field will need to be altered [8, 9]. A new mechanism driving inflation, such as multiple interacting fields or other exotic will need to be adopted.

Past attempts of measuring non-Gaussianity in the CMB have been to use the bispectrum and associated three-point correlation function or N-point distribution functions to determine deviations from Gaussianity. The first-order deviations are parameterized by the primordial non-Gaussianity parameter f_{NL} (eq. 1). Such stud-

ies have found f_{NL} to be consistent with zero [10–13].

In this analysis we use the trispectrum, or the four-point correlation function of temperature anisotropies, to measure primordial non-Gaussianity using WMAP 5-year data [14]. The trispectrum has the advantage that it can be used to uncover a cubic-order departure from a Gaussian field. This second-order departure, parameterized by either g_{NL} of f_{NL}^2 , has never been before measured using the CMB trispectrum. A measurement of f_{NL}^2 in the trispectrum puts a direct constraint on τ_{NL} , an important parameter for many inflationary models, through the relation $\tau_{\text{NL}} = 36f_{\text{NL}}^2/25$ [16]. An observational constraint on this parameter is important since it is possible to construct reasonable inflationary models that produce a negligible f_{NL} in the bispectrum but a detectable non-zero τ_{NL} in the trispectrum [15].

Theory.—To parameterize the non-Gaussianity of a nearly Gaussian field, such as the primordial curvature perturbations $\Phi(\mathbf{x})$, we can expand it perturbatively [17] to second order as:

$$\Phi(\mathbf{x}) = \phi_L(\mathbf{x}) + f_{\text{NL}} [\phi_L^2(\mathbf{x}) - \langle \phi_L(\mathbf{x}) \rangle^2] + g_{\text{NL}} \phi_L^3(\mathbf{x}) \quad (1)$$

where $\phi_L(\mathbf{x})$ is the purely Gaussian part and f_{NL} and g_{NL} parametrize the first and second order deviations from Gaussianity. Fortunately, information about the curvature perturbations are contained within the CMB through the spherical harmonic coefficients of the temperature anisotropies:

$$a_{lm} = 4\pi(-i)^l \int \frac{d^3\mathbf{k}}{(2\pi)^3} \Phi(\mathbf{k}) g_{Tl}(k) Y_l^{m*}(\hat{\mathbf{k}}) \quad (2)$$

$$\theta(\hat{\mathbf{n}}) = \frac{\delta T}{T}(\hat{\mathbf{n}}) = \sum_{lm} a_{lm} Y_l^{m*}(\hat{\mathbf{n}}), \quad (3)$$

where $\Phi(\mathbf{k})$ are the primordial curvature perturbations, g_{Tl} is the radiation transfer function that gives the angular power spectrum as $C_l = (2/\pi) \int k^2 dk P_\Phi(k) g_{Tl}^2(k)$, θ

*jsmidt@uci.edu

is the field of temperature fluctuations in the CMB and Y_m^l 's are the spherical harmonics.

In order to extract the first and second order deviations from Gaussianity it is useful to consider the trispectrum of the CMB, which conveniently breaks into a Gaussian and non-Gaussian or connected piece:

$$\begin{aligned} \langle a_{l_1 m_1} a_{l_2 m_2} a_{l_3 m_3} a_{l_4 m_4} \rangle &= \\ \langle a_{l_1 m_1} a_{l_2 m_2} a_{l_3 m_3} a_{l_4 m_4} \rangle_G &+ \langle a_{l_1 m_1} a_{l_2 m_2} a_{l_3 m_3} a_{l_4 m_4} \rangle_c \end{aligned} \quad (4)$$

where the connected part of the trispectrum can be expanded as [17]

$$\begin{aligned} \langle a_{l_1 m_1} a_{l_2 m_2} a_{l_3 m_3} a_{l_4 m_4} \rangle_c &= \\ \sum_{LM} (-1)^M T_{l_1 l_2}^{l_3 l_4}(L) \begin{pmatrix} l_1 & l_2 & L \\ m_1 & m_2 & M \end{pmatrix} \begin{pmatrix} l_3 & l_4 & L \\ m_3 & m_4 & -M \end{pmatrix} & (5) \\ T_{l_3 l_4}^{l_1 l_2}(L) &= 4f_{\text{NL}}^2 h_{l_1 l_2 L} h_{l_3 l_4 L}^* \\ \int r_1^2 dr_1 r_2^2 dr_2 F_L(r_1, r_2) \alpha_{l_1}(r_1) \beta_{l_2}(r_1) \alpha_{l_3}(r_2) \beta_{l_4}(r_2) & (6) \\ + g_{\text{NL}} h_{l_1 l_2 L} h_{l_3 l_4 L}^* & \\ \int r^2 dr \beta_{l_2}(r) \beta_{l_4}(r) [\mu_{l_1}(r) \beta_{l_3}(r) + \mu_{l_3}(r) \beta_{l_1}(r)] & \end{aligned}$$

with the quantity in parenthesis being the Wigner-3j symbols, and $h_{l_1 l_2 l_3}$ is defined such that

$$h_{l_1 l_2 l_3} = \sqrt{\frac{(2l_1 + 1)(2l_2 + 1)(2l_3 + 1)}{4\pi}} \begin{pmatrix} l_1 & l_2 & l_3 \\ 0 & 0 & 0 \end{pmatrix}. \quad (7)$$

and

$$\alpha_l(r) \equiv \frac{2}{\pi} \int k^2 dk g_{Tl}(k) j_l(kr), \quad (8)$$

$$\beta_l(r) \equiv \frac{2}{\pi} \int k^2 dk P_\Phi(k) g_{Tl}(k) j_l(kr), \quad (9)$$

$$\mu_l(r) \equiv \frac{2}{\pi} \int k^2 dk g_{Tl}(k) j_l(kr) \quad (10)$$

Here, $P_\Phi(k) \propto k^{n_s - 4}$ is the primordial power spectrum of curvature perturbations, $g_{Tl}(k)$ is defined above, $j_l(kr)$ are the spherical bessel functions and r parameterizes the line of sight. The Gaussian piece of the trispectrum [14] is similarly defined by equation (5) with $T_{l_1 l_2}^{l_3 l_4}(L)$ exchanged by $G_{l_1 l_2}^{l_3 l_4}(L)$ defined as

$$\begin{aligned} G_{l_1 l_2}^{l_3 l_4}(L) &= (-1)^{l_1 + l_3} \sqrt{(2l_1 + 1)(2l_2 + 2)} C_{l_1} C_{l_3} \delta_{L0} \delta_{l_1 l_2} \delta_{l_3 l_4} \\ &(2L + 1) C_{l_1} C_{l_2} [(-1)^{l_2 + l_3 + L} \delta_{l_1 l_3} \delta_{l_2 l_4} + \delta_{l_1 l_4} \delta_{l_2 l_3}] \end{aligned} \quad (11)$$

where C_l is the temperature power spectrum.

To calculate the quantities above from partial sky maps of temperature fluctuations we form the four point esti-

mators [18]:

$$\begin{aligned} \mathcal{K}_i^{(3,1)} &= 4f_{\text{NL}}^2 \int r_1^2 dr_1 \int r_2^2 dr_2 \mathcal{J}_i^{ABA,B}(r_1, r_2) \quad (12) \\ &+ 2g_{\text{NL}} \int r^2 dr \mathcal{L}_i^{MB^2,B}(r) \end{aligned}$$

$$\begin{aligned} \mathcal{K}_i^{(2,2)} &= 4f_{\text{NL}}^2 \int r_1^2 dr_1 \int r_2^2 dr_2 \mathcal{J}_i^{AB,AB}(r_1, r_2) \quad (13) \\ &+ 2g_{\text{NL}} \int r^2 dr \mathcal{L}_i^{MB^2,B}(r) \end{aligned}$$

where $\mathcal{J}_i^{ABA,B}(r_1, r_2)$, $\mathcal{L}_i^{MB^2,B}(r)$, $\mathcal{J}_i^{AB,AB}(r_1, r_2)$, and $\mathcal{L}_i^{MB^2,B}(r)$ are the angular power spectra of their respective maps. For example $\mathcal{L}_i^{MB^2,B}(r)$ is defined as:

$$\mathcal{L}_i^{MB^2,B}(r) = \frac{1}{2l+1} \sum_m (MB^2)_{lm} B_{lm}^*. \quad (14)$$

Here the maps A , B and M are maps optimized for the detection of primordial non-Gaussianity defined as:

$$A(r, \Omega) = \sum_{lm} A_{lm} Y_{lm}(\Omega); \quad A_{lm} = \frac{\alpha_{lm}}{C_l} a_{lm} \quad (15)$$

$$B(r, \Omega) = \sum_{lm} B_{lm} Y_{lm}(\Omega); \quad B_{lm} = \frac{\beta_{lm}}{C_l} a_{lm} \quad (16)$$

$$M(r, \Omega) = \sum_{lm} M_{lm} Y_{lm}(\Omega); \quad M_{lm} = \frac{\mu_{lm}}{C_l} a_{lm} \quad (17)$$

These estimators can be related to the above calculation for the trispectrum as:

$$\mathcal{K}_i^{(2,2)} = \frac{1}{(2l+1)} \sum_{l_i} \frac{1}{(2l+1)} \frac{T_{l_1 l_2}^{l_3 l_4}(l) \hat{T}_{l_3 l_4}^{l_1 l_2}(l)}{C_{l_1} C_{l_2} C_{l_3} C_{l_4}}; \quad (18)$$

$$\mathcal{K}_i^{(3,1)} = \frac{1}{(2l+1)} \sum_{l_i L} \frac{1}{(2L+1)} \frac{T_{l_3 l_4}^{l_1 l_2}(L) \hat{T}_{l_3 l_4}^{l_1 l_2}(L)}{C_{l_1} C_{l_2} C_{l_3} C_l}. \quad (19)$$

where the C_l 's in the denominator contains the theoretical spectrum plus noise $C_l = C_l^T + C_l^N$.

Analysis and Results.—First we calculate $T_{l_1 l_2}^{l_3 l_4}(L)$ and $G_{l_1 l_2}^{l_3 l_4}(L)$ using equations (5-11). To obtain C_l we use CAMB [19]¹ using the WMAP 5-year best fit parameters and use the beam transfer functions from the WMAP team. Furthermore we obtain α , β , μ and F using a modified version of the CMBFAST code [20]². Plots of many of these quantities can be found in Ref. [13].

Once we have $T_{l_1 l_2}^{l_3 l_4}(L)$ and $G_{l_1 l_2}^{l_3 l_4}(L)$ we calculate the theoretical estimators $\mathcal{K}_i^{3,1}$ and $\mathcal{K}_i^{2,2}$ for a model with f_{NL} and $g_{\text{NL}} = 1$. The righthand sides of these estimators, eq. 18 and 19, can be broken up into two pieces, the

¹ <http://camb.info/>

² <http://www.cfa.harvard.edu/mzaldarr/CMBFAST/cmbfast.html>

first being proportional to f_{NL}^2 and the second being proportional to g_{NL} . These are plotted in Figure 1. These curves are compared with estimators derived from data to determine the magnitude of each statistic. Since we have two estimators, we can solve for the two unknowns f_{NL}^2 and g_{NL} by fitting both estimators simultaneously.

To calculate³ the estimators from data, used in the lefthand side of equations (18) and (19), we use both the raw and foreground-cleaned WMAP 5-Year Stokes I maps for V- and W-bands masked with the KQ75 mask⁴. We use Healpix to analyze the maps. For this analysis we only considered data out to $l_{\text{max}} = 600$.

Our recipe for obtaining $K_l^{(3,1)}$ and $K_l^{(2,2)}$ from data:

1. Use Healpix to generate a_{lm} from the masked WMAP 5-year Stokes-I Sky Maps for the V and W frequency bands.
2. Obtain $A(r, \Omega)$, $B(r, \Omega)$ and $M(r, \Omega)$ from equations (15), (16), and (17) by using $\alpha(r)$, $\beta(r)$ and $\mu(r)$ from equation (8) and (9), respectively with the a_{lm} obtained from the maps.
3. Calculate $J_l^{ABA,B}$, $\mathcal{L}_l^{MB^2,B}$, $J_l^{AB,AB}$ and $\mathcal{L}_l^{B^2,BM}$ from equations (14-17) noting the full details in [18]. We integrate over r from $\tau = 0.004$ to 2 with 25 steps.
4. Calculate the estimators K_l^{3-1} and K_l^{2-2} for each frequency band using equations (12) and (13) and dividing by f_{sky} to compensate for the masked sky.

Figure 1 shows the results for $\mathcal{K}_l^{3,1}$ and $\mathcal{K}_l^{2,2}$ for the V and W frequency bands extracted from the raw WMAP 5-Year maps.

In order to do proper statistics for our data fitting we create 250 simulated Gaussian maps of each frequency band with $n_{\text{side}} = 512$. To obtain Gaussian maps we run the *synfast* routine of Healpix with an in-file representing the WMAP 5-year best-fit CMB anisotropy power spectrum and generate maps with information out to $l = 600$. We then use *anafast*, without employing an iteration scheme, masking with the KQ75 mask, to produce a_{lm} 's for the Gaussian maps out to $l = 600$. Obtaining estimators from these Gaussian maps allows us to uncover the Gaussian contribution to each estimator in addition to providing us information needed to calculate the error bars on our results.

This whole process is computationally intensive. To calculate all theoretical estimators took nearly 8,000 CPU hours. Furthermore, all the estimators from Gaussian and data maps combined took an additional 1600 CPU hours.

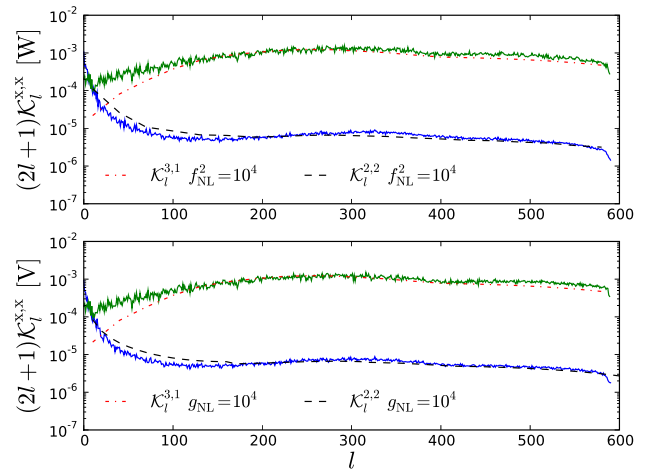


FIG. 1: The top plot shows the $\mathcal{K}_l^{3,1}$ and $\mathcal{K}_l^{2,2}$ estimators, shown in green and blue respectively, taken from data for the W band. The same estimators for the V band are shown on the bottom. Additionally on the top the theoretical contributions for $\mathcal{K}_l^{2,2}$ and $\mathcal{K}_l^{3,1}$ proportional to f_{NL} are shown with the bottom showing those proportional to g_{NL} . The Gaussian contributions were not removed from these plots.

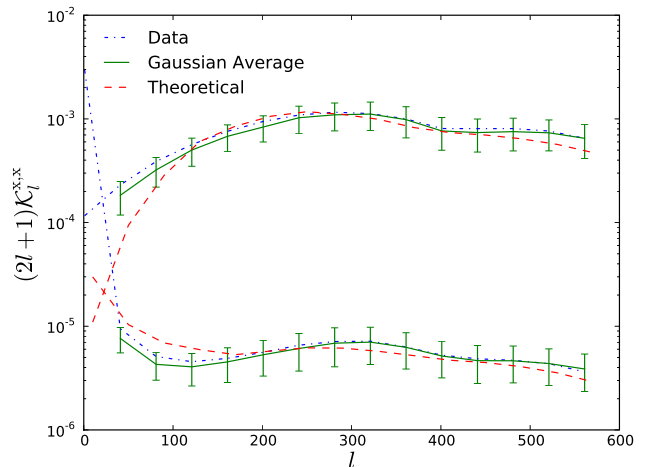


FIG. 2: The relation between the full estimators coming from data versus the Gaussian contributions. The green curve show the Gaussian contributions coming from averaging the estimators from the Gaussian maps. The red curve is the theoretical Gaussian piece calculated from Eq. 11 using the WMAP-5 best-fit cosmology power spectrum. The error bars show one standard deviation from the Gaussian curves. These curves are from W band data.

As previously discussed, the full trispectrum can be decomposed into both a Gaussian and non-Gaussian or connected piece. To make a measurement of non-Gaussianity we to subtract off the Gaussian piece from the full trispectrum. Figure 2 shows the the relationship between the full trispectrum and the Gaussian piece. In this plot the Gaussian piece was calculated in two different ways as a sanity check. First, the Gaussian maps were averaged

³ see Smidt et al. 2009 for a similar calculation using the bispectrum for more details. [13]

⁴ <http://lambda.gsfc.nasa.gov/>

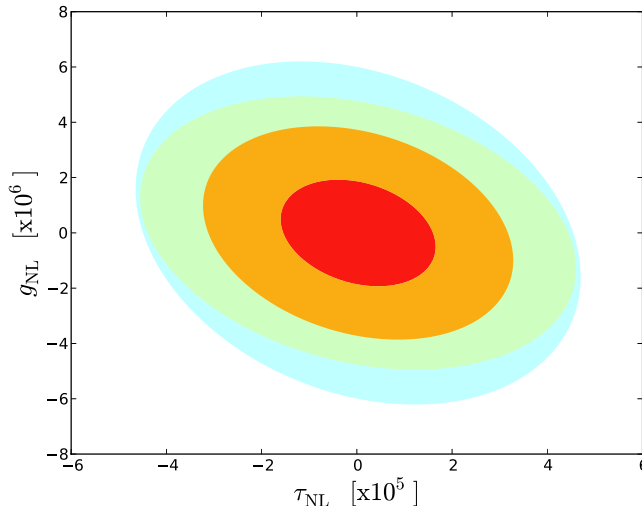


FIG. 3: The 95% confidence levels for g_{NL} versus τ_{NL} . The red and orange represent the 68% and 95% intervals respectively for the combined V+W analysis. The light blue regions represent the 95% confidence intervals for the V band analysis, and the light green regions are for the W band.

Band	W	V	V+W
Raw			
$\sqrt{f_{\text{NL}}^2}$	42 ± 397	44 ± 402	43 ± 337
g_{NL}	$4.3 \times 10^4 \pm 2.5 \times 10^6$	$3.6 \times 10^4 \pm 3.1 \times 10^6$	$4.0 \times 10^4 \pm 1.9 \times 10^6$
τ_{NL}	$2.7 \times 10^4 \pm 2.3 \times 10^5$	$2.7 \times 10^4 \pm 2.3 \times 10^5$	$2.7 \times 10^4 \pm 1.6 \times 10^5$
FC			
$\sqrt{f_{\text{NL}}^2}$	43 ± 399	44 ± 403	43 ± 336
g_{NL}	$4.2 \times 10^4 \pm 2.5 \times 10^6$	$3.7 \times 10^4 \pm 3.1 \times 10^6$	$3.9 \times 10^4 \pm 1.9 \times 10^6$
τ_{NL}	$2.7 \times 10^4 \pm 2.3 \times 10^5$	$2.7 \times 10^4 \pm 2.3 \times 10^5$	$2.7 \times 10^4 \pm 1.6 \times 10^5$

TABLE I: Results for each frequency band to 1σ . Values for $\sqrt{f_{\text{NL}}^2}$, g_{NL} and τ_{NL} on the top are for raw maps. The values on the bottom are for foreground clean maps.

over. Second, the Gaussian piece of each estimator is calculated using the WMAP-5 best-fit power spectrum in Eq. 11 replacing $\hat{T}_{l_1 l_2}^{l_3 l_4}(L)$ with $\hat{G}_{l_1 l_2}^{l_3 l_4}(L)$ in Eq. 18 and 19.

Another important observation must be said. As seen in Fig. 2, the difference between the Gaussian piece of each estimator and the full estimator coming from data is a few percent. In order to obtain a detection one would need to have numerical routines with sub-percent accuracy. Such precision in the simulations is not a requirement for the current work as we do not find a non-zero detection of g_{NL} or τ_{NL} , but in future, the accuracy of numerical codes may limit the precision of a measurement of these quantities.

After obtaining the theory, data and simulated curves we use the best fitting procedure described in [13] where we minimize χ^2 to fit f_{NL}^2 and g_{NL} simultaneously, constraining τ_{NL} by f_{NL}^2 as discussed above. Our results are listed in Table I. We see that $\sqrt{f_{\text{NL}}^2}$, g_{NL} and τ_{NL} are consistent with zero with 95% confidence level ranges

$-631 < \sqrt{f_{\text{NL}}^2} < 717$, $-3.80 < g_{\text{NL}}/10^6 < 3.88$ and from f_{NL}^2 , $-3.2 < \tau_{\text{NL}}/10^5 < 3.3$ for V+W-band in foreground-cleaned maps. The 95% confidence intervals of g_{NL} versus τ_{NL} are plotted in Figure 3 for each band.

The constraint on τ_{NL} is a significant improvement over the previous constraint of $\tau_{\text{NL}} < 10^8$ based on null detections of the trispectrum from COBE [16, 22, 23]. Our limit on τ_{NL} from WMAP 5-year data at $\tau_{\text{NL}} < 3.3 \times 10^5$ is close to a level where interesting constraints can started to be placed on models available in the literature for primordial perturbations, such as due to cosmic strings [24]. This is the first direct limit on this cubic-order non-Gaussianity parameter with the CMB trispectrum.

We are grateful to Eiichiro Komatsu, and Kendrick Smith for assistance during various stages of this work. This work was supported by NSF CAREER AST-0645427 and NASA NNX10AD42G at UCI and STFC rolling grant ST/G002231/1 (DM).

-
- [1] A. H. Guth, Phys. Rev. D **23**, 347 (1981).
 - [2] A. D. Linde, Phys. Lett. B **108**, 389 (1982).
 - [3] A. J. Albrecht and P. J. Steinhardt, Phys. Rev. Lett. **48**, 1220 (1982).
 - [4] A. H. Guth and S. Y. Pi, Phys. Rev. Lett. **49**, 1110 (1982).
 - [5] J. M. Bardeen, P. J. Steinhardt and M. S. Turner, Phys. Rev. D **28**, 679 (1983).
 - [6] S. W. Hawking, Phys. Lett. B **115**, 295 (1982).
 - [7] V. F. Mukhanov, H. A. Feldman and R. H. Brandenberger, Phys. Rept. **215**, 203 (1992).
 - [8] N. Bartolo, E. Komatsu, S. Matarrese and A. Riotto, Phys. Rept. **402**, 103 (2004)
 - [9] E. Komatsu *et al.*, arXiv:0902.4759 [astro-ph.CO].
 - [10] A. P. S. Yadav and B. D. Wandelt, Phys. Rev. Lett. **100**, 181301 (2008)
 - [11] E. Komatsu *et al.* [WMAP Collaboration], Astrophys. J. Suppl. **180**, 330 (2009)
 - [12] K. M. Smith, L. Senatore and M. Zaldarriaga, arXiv:0901.2572 [astro-ph].
 - [13] J. Smidt, A. Amblard, P. Serra and A. Cooray, Phys. Rev. D **80**, 123005 (2009)
 - [14] W. Hu, Phys. Rev. D **64**, 083005 (2001)
 - [15] M. Zaldarriaga, Private communication (2010).
 - [16] L. Boubekur and D. H. Lyth, Phys. Rev. D **73**, 021301 (2006)
 - [17] N. Kogo and E. Komatsu, Phys. Rev. D **73**, 083007 (2006)
 - [18] D. Munshi, A. Heavens, A. Cooray, J. Smidt, P. Coles and P. Serra, arXiv:0910.3693 [astro-ph.CO].
 - [19] A. Lewis, A. Challinor and A. Lasenby, Astrophys. J. **538**, 473 (2000)
 - [20] U. Seljak and M. Zaldarriaga, Astrophys. J. **469**, 437 (1996)
 - [21] D. Jeong and E. Komatsu, Astrophys. J. **703**, 1230 (2009)
 - [22] M. Kunz *et al.* ApJL 563, L99 (2001)
 - [23] E. Komatsu, arXiv:astro-ph/0206039.
 - [24] K. T. Engel, K. S. M. Lee and M. B. Wise, Phys. Rev. D **79**, 103530 (2009)